Available online at www.sciencedirect.com
ScienceDirect
Trans. Nonferrous Met. Soc. China 28(2018) 2181−2189
Transactions of Nonferrous Metals Society of China
www.tnmsc.cn

Corrosion performance of high pressure die-cast Al−6Si−3Ni and Al−6Si−3Ni−2Cu alloys in aqueous NaCl solution

Srinivasan ARTHANARI, Jae Cheol JANG, Kwang Seon SHIN

Research Institute of Advanced Materials, School of Materials Science and Engineering, Seoul National University, Gwanak-gu, Seoul 08826, Korea

Received 12 January 2018; accepted 23 July 2018

Abstract: The corrosion performance of high pressure die-cast Al−6Si−3Ni (SN63) and Al−6Si−3Ni−2Cu (SNC632) alloys in 3.5% (mass fraction) NaCl solution was investigated. X-ray diffraction (XRD) and microstructural studies revealed the presence of single phase Si and binary Al_3Ni/Al_3Ni_2 phases along the grain boundary. Besides, the single Cu phase was also identified at the grain boundaries of the SNC632 alloy. Electrochemical corrosion results revealed that, the SNC632 alloy exhibited nobler shift in corrosion potential (φ_{corr}), lower corrosion current density (J_{corr}) and higher corrosion resistance compared to the SN63 alloy. Equivalent circuit curve fitting analysis of electrochemical impedance spectroscopy (EIS) results revealed the existence of two interfaces between the electrolyte and substrate. The surface layer and charge transfer resistance (R_{ct}) of the SNC632 alloy was higher than that of the SN63 alloy. Immersion corrosion test results also confirmed the lower corrosion rate of the SNC632 alloy and substantiated the electrochemical corrosion results. Cu addition improved the corrosion resistance, which was mainly attributed to the absence of secondary Cu containing intermetallic phases in the SNC632 alloy and Cu presented as single phase.
Key words: die-casting; aluminum alloys; corrosion; polarization; electrochemical impedance spectroscopy (EIS)

1 Introduction

Aluminum (Al) alloys are mainly used as structural materials in the automotive and aerospace industries owing to their several advantages such as formability, high electrical and thermal conductivity and low density (2.7 g/cm^3) [1−4]. Controlling the alloying composition generally improves the mechanical properties by forming several hard intermetallic phases. Besides, the processing conditions also significantly alter the alloy properties. Nevertheless, achieving high strength alloy without compromising the chemical properties is a challenging task. Aluminum alloys possess relatively better corrosion resistance since the oxide layer formed (2−10 nm in thickness) on the alloy surface is stable and Al is also thermodynamically stable in the pH range of 5−8.5. However, the corrosion resistance is severely affected by the addition of alloying elements. Mechanical properties of Al alloys can be improved by the addition of alloying elements. Silicon (Si) is one of the most vital and commonly used elements (5%−17%, mass fraction) in aluminum alloys to improve the fluidity and reduce the shrinkage [5,6]. Si addition substantially lowers the melting point without affecting the brittleness of the resulting alloy, which is favorable for casting of Al alloys in the industries [7]. However, higher Si content reduces its thermal expansion co-efficient, machinability and corrosion behavior [8,9].

Nickel (Ni) is also used as one of the common alloying elements to Al−Si based alloys to improve their hot hardness and the distribution of large volume of nickel aluminides such as Al_3Ni and Al_3Ni_2 [10]. Furthermore, the amount of intermetallic Al_3Ni/Al_3Ni_2 phases increases as the Ni content is increased, and the compression, strength and hardness at elevated temperatures and flexion resistance are improved [11]. However, the presence of Al_3Ni/Al_3Ni_2 phases is detrimental to corrosion [12−14]. Binary AlNi phases have more noble potential compared to α(Al) matrix, thus accelerates the Al dissolution [15−17]. Cu addition generally improves the strength of Al−Si based alloys at elevated temperature. Cu has good solubility and significant strengthening effect by solid solution strengthening and dispersion strengthening mechanisms [18−20]. Mechanical properties and high temperature properties of Al−Si alloys can be improved by altering the alloying element composition; however, there are possibilities to

Corresponding author: Kwang Seon SHIN; E-mail: ksshin@snu.ac.kr
DOI: 10.1016/S1003-6326(18)64863-0

alter the corrosion behavior. Addition of Ni and Cu to the Al−Si based alloys could improve the mechanical properties. Nevertheless, they alter the corrosion properties and need to be investigated. Recently, we have reported the corrosion behavior of Al−Si−Ni (SN) and Al−Si−Ni−Cu (SNC) alloys of lower Si content with varying Ni. The corrosion resistance was improved as the Cu was added to the SN31 alloy; however, increase in Ni content decreased the corrosion resistance due to the presence of higher amount of Al_3Ni phase [21]. High pressure die-cast Al alloys with higher Si contents (Al−6Si−3Ni (SN63) and Al−6Si−3Ni−2Cu (SNC632)) were developed to improve the mechanical and thermal conductivity; however, their corrosion behavior was less investigated. Therefore, in the present investigation, we evaluate the corrosion behavior of SN63 and SNC632 alloys in 3.5% (mass fraction) NaCl solution. Corrosion performance was assessed using electrochemical studies including open circuit potential (OCP) measurement, electrochemical impedance spectroscopy (EIS) and potentiodynamic polarization and immersion corrosion tests were also performed to substantiate the electrochemical corrosion results. Surface morphologies of corroded alloys after 72 h immersion were also observed to reveal the corrosion morphologies, and were compared with corrosion results.

2 Experimental

2.1 Alloy preparation and microstructural characterization

SN63 (6.0% Si, 3.0% Ni and balance Al, molar fraction) and SNC632 (6.0% Si, 3.0% Ni, 2% Cu and balance Al, molar fraction) were prepared using a 125 t die-casting machine BD−125V5EX (TOYO Co. Ltd.) and the detailed procedure was reported in our previous work [22] and briefly described here for understanding. During the casting process, the mold was initially pre-heated at 200 °C, the plunger inner diameter was 40 mm and the casting was carried out at the plunger speed of 0.2 m/s (initial speed) and 2.0 m/s (fastest speed). The specimens for the analysis were sliced from the biscuit (ASTM−E8 Standard). Bruker D8 Advance instrument with Cu K_α radiation in the 2θ range of 20°−80° at a scan rate of 2 (°)/min was used for the XRD studies. Microstructures were observed using a ZEISS Merlin Compact field emission-scanning electron microscope (FE-SEM) attached with an energy dispersive X-ray analyzer (EDAX) at an accelerating voltage of 15 kV. Prior to SEM observation, alloys were abraded using silicon carbide (SiC) emery papers up to 2000$^{\#}$ followed by mirror polished with 0.05 μm alumina (Al_2O_3), ultra-sonicated and air dried.

2.2 Corrosion evaluation of SN63 and SNC632 alloys

Corrosion performance of SN63 and SNC632 alloys (15 mm × 10 mm × 3 mm) was evaluated using electrochemical and immersion corrosion tests and detailed experimental procedure can be found elsewhere [22]. Alloys from the cast biscuits were sliced and abraded with silicon carbide (SiC) emery papers (2000$^{\#}$) followed by ultrasonic cleaning and air drying. A Princeton applied research (PAR) VersaStat 3 electrochemical workstation was used for electrochemical corrosion tests. Working electrode (Al alloy, 1 cm^2) was exposed to 3.5% (mass fraction) NaCl solution for 30 min to establish the stable OCP with respect to Ag/AgCl reference electrode. Platinum (Pt) sheet (~3 cm^2) was used as counter electrode. EIS studies were carried out at OCP in the frequency range between 100 kHz and 0.05 Hz with the amplitude of 10 mV. Potentiodynamic polarization tests were carried out in the potential range of OCP±250 mV. Samples for immersion corrosion tests were also prepared using same procedure and immersed for 72 h in 3.5% NaCl solution. The mass loss before and after corrosion tests and hydrogen volume during exposure were also measured to calculate the corrosion rates, and the detailed procedure is given in our earlier work [22]. Duplicate experiments were also performed to confirm the reproducibility of the results. FE-SEM surface morphologies and EDAX results were observed after 72 h of immersion tests.

3 Results and discussion

3.1 Microstructures of SN63 and SNC632 alloys

XRD patterns of the SN63 and SNC632 alloys are shown in Fig. 1. XRD patterns clearly indicated the presence of α(Al), Al_3Ni, Al_3Ni_2, pure Si and Cu phases, and the peaks matched well with our previous work [21]. The presence of Al_3Ni phase (ICDD−04-007-0402) was confirmed for both the SN63 and SNC632 alloys. However, in addition to the Al_3Ni phase, Al_3Ni_2 phase

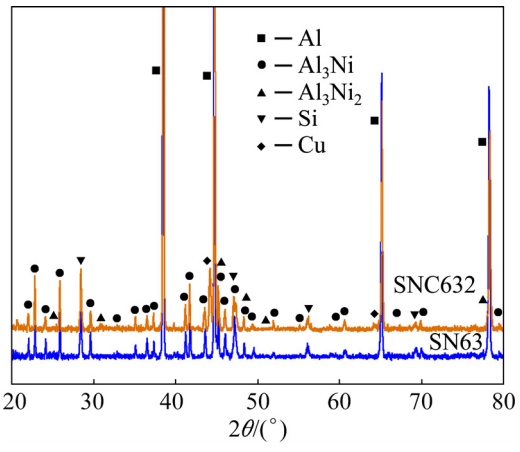

Fig. 1 XRD patterns of SN63 and SNC632 alloys

(ICDD−00-014-0648) was also identified for the SNC632 alloy and these peaks were not noticed for the SN63 alloy. The pure Si peaks were confirmed at 2θ=28.49°, 47.04°, 56.02°, 68.99° and 76.08° (ICDD−00-001-0787). Cu addition to SN63 alloy resulted in the precipitation of pure Cu phases (ICDD−01-080-5762) at the grain boundaries and any Al-contained intermetallic phases did not form, which was confirmed from the XRD patterns. These results were also confirmed by the thermodynamic calculation results. The high intensity peaks are attributed to the α(Al) (ICDD−00-001-1180).

Figure 2 shows the FE-SEM images and EDAX elemental distribution maps of SN63 and SNC632 alloys. It is seen that fiber- and rod-like precipitates are identified at the grain boundaries of SN63 and SNC632 alloys. These phases could be attributed to binary Al_3Ni/Al_3Ni_2 phases. Furthermore, EDAX elemental distribution also clearly indicated that, Si is also presented at the grain boundaries (Fig. 2(a)). It has been reported that, Si can be identified as single phase in Al alloys since it has lower solubility in aluminum [1]. In SNC632 alloy, the distribution of Al_3Ni/Al_3Ni_2 phases was also confirmed.

In addition, the distribution of Cu at the grain boundaries was also evident (Figs. 2(b) and 3). Cu with lower addition could dissolve in aluminum matrix [23] and hence the precipitation of secondary phase of AlCu was not noticed. These results further substantiated these by the XRD results and thermodynamic calculation.

3.2 Corrosion performance of SN63 and SNC632 alloys

Corrosion performance of SN63 and SNC632 alloys was evaluated in 3.5% NaCl solution using electrochemical and immersion corrosion tests. Figure 4(a) shows the change in OCP values of SN63 and SNC632 alloys. It can be seen from the results that, Cu addition shifted the OCP value from −0.611 (SN63) to −0.568 V (SNC632), indicating the nobility of SNC632 alloy. Shift in OCP value of about 40 mV is attributed to the formation of stable surface layer which could control the further reaction of underneath surface.

Potentiodynamic polarization curves of SN63 and SNC632 alloys after 1800 s of exposure are compared in Fig. 4(b). Polarization parameters were also extracted using Tafel extrapolation method from the polarization curves. Corrosion potential (φ_{corr}) values were −0.618 and −0.566 V for the SN63 and the SNC632 alloys, respectively, and these results are in good agreement with the OCP values. The positive shift in φ_{corr} value of SNC632 indicated that, the Cu-contained alloy had the stable surface layer in corrosive solution, which could control the penetration of aggressive ions into the surface layer. Corrosion current density (J_{corr}) value of the SNC632 alloy ((4.07±0.38) μA/cm^2) was lower than that of the SN63 alloy ((5.68±0.62) μA/cm^2), indicating its better corrosion resistance. Cathodic and anodic corrosion current densities of SNC632 were also lower than those of SN63 alloy, indicating the reduction of anodic and cathodic reaction kinetics.

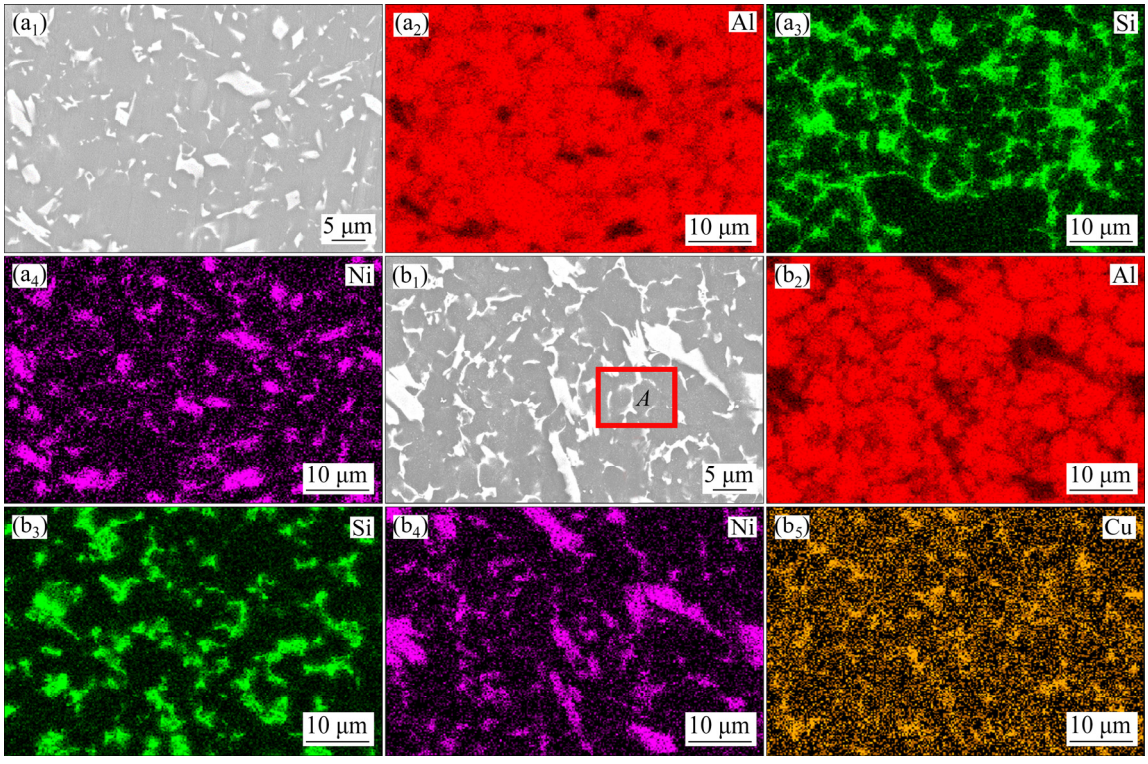

Fig. 2 Microstructures and EDAX elemental distributions of SN63 (a) and SNC632 (b) alloys

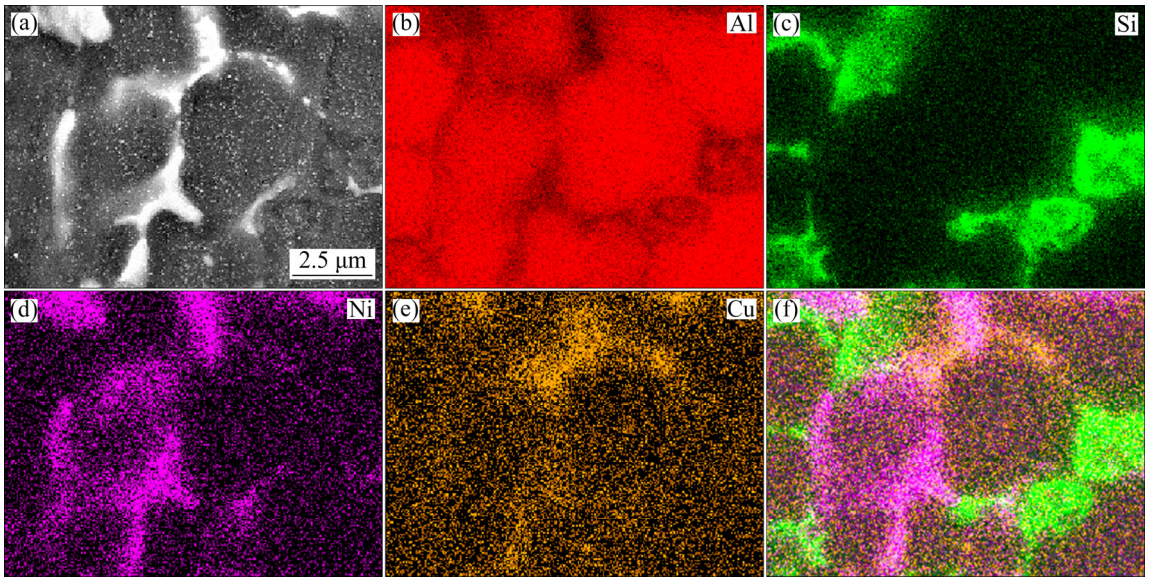

Fig. 3 Microstructures and EDAX elemental distributions of Zone *A* in Fig. 2(b_1) ((f) shows combined image of (c), (d) and (e))

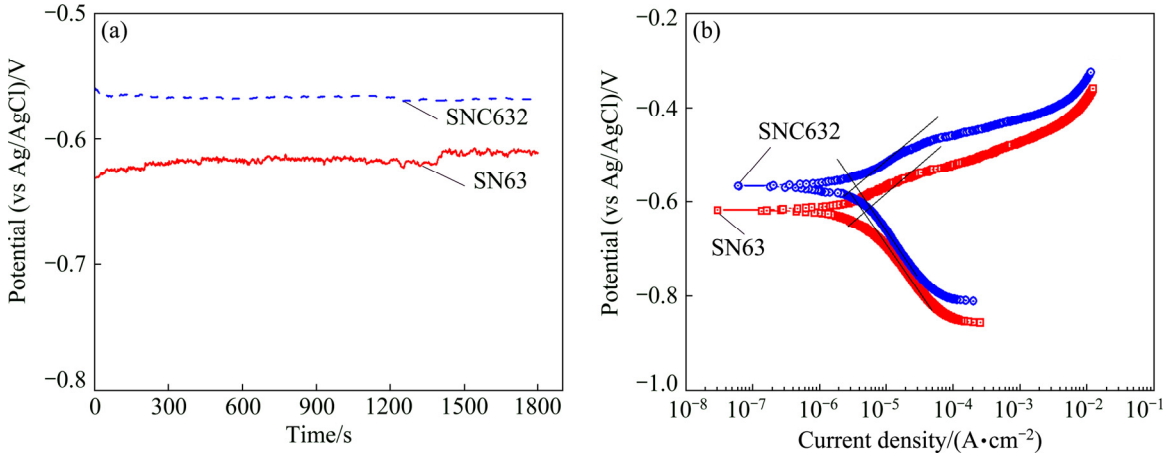

Fig. 4 Change in OCP values (a) and potentiodynamic polarization curves (b) of SN63 and SNC632 alloys in 3.5% NaCl solution

It has been reported that, the cooling rate has an important role in the microstructure, and corresponding properties (e.g. corrosion behavior or mechanical strength) [24−26] of Al−Cu−Si alloys. Although the cooling rate was not focused in this work, it is considered that similar microstructural features (dendritic spacing of about 15 μm) are compared, as depicted in Fig. 2. Considering Al−Cu [26] and Al−Ni [27] based alloys, it is recognized that eutectic morphology containing intermetallic compounds (IMCs), e.g., Al_2Cu [24−26] and Al_3Ni [27], affects significantly the anode-to-cathode (A_a/A_c) area ratios, and consequently the corrosion behavior. From the electrochemical point of view, the galvanic couple between these two distinctive constituent phases is strongly dependent of the distance and geometry (morphology) [28], which affects the corrosion kinetics but not its mechanism. Additionally, it has also been reported that distribution and morphology of these IMCs have also important role in the corrosion behavior. A eutectic mixture containing interconnected and non-interconnected Al_3Ni IMC particles has distinctive A_a/A_c and corresponding corrosion resistances are drastically different, as previously reported [27].

Electrochemical corrosion behaviors of the SN63 and SN632 alloys were also evaluated using EIS studies to understand the corrosion mechanism. Figures 5(a) and (b) show the EIS Nyquist and Bode plots, respectively. It can be seen from Fig. 5(a) that, both SN63 and SNC632 alloys exhibited two depressed capacitive loops. Capacitive loop appearing at high and low frequency regions are attributed to the electrolyte/surface layer and surface layer/substrate interfaces, respectively. Capacitive loop diameters of SNC632 alloy were larger compared to those of the SN63 alloy, indicating the better capacitive behavior and higher charge transfer resistance. Direct relationship between the applied frequency and impedance ($|Z|$) (phase angle) values can be identified from the Bode plots (Fig. 5(b)). The $|Z|$ of

the SNC632 alloy increased as the frequency reached 0.05 Hz with two slopes and the value remained higher compared to that of the SN63 alloy, indicating its better corrosion resistance. Bode phase angle plots (Fig. 5(b)) consisted of two peaks (1×10^3−1 and 1−0.05 Hz) and the phase angle maxima and peak areas of the SNC632 were marginally larger compared to those of SN63 alloy, which is attributed to the capacitive behavior and higher corrosion resistance. EIS results were curve fitted with electrical equivalent circuit (EC) and EC model is depicted in Fig. 6 and the fitted parameters are included in Table 1.

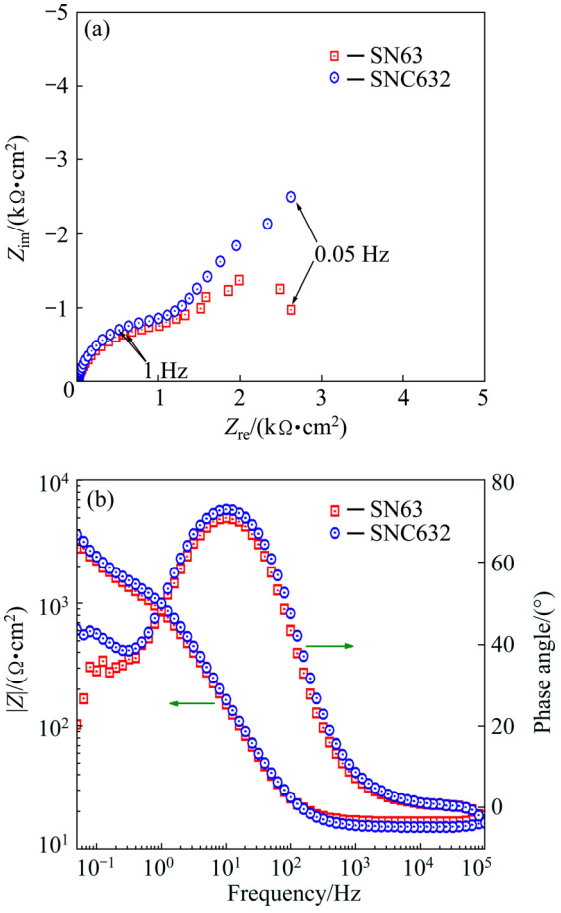

Fig. 5 EIS Nyquist (a) and Bode plots (b) of SN63 and SNC632 alloys in 3.5% NaCl solution after 1800 s

Constance phase elements (Q) have been used in the EC instead of capacitance (C) to indicate the deviation from the ideal capacitive behavior and the exponent n has been used to show the closeness of the experimental results to the ideal behavior [14,29]. R_1 and R_2 values of the SNC632 alloy were higher compared to those of the SN63 alloy, and furthermore, Q_1 and Q_2 values were lower for the SNC632 alloy compared to those for the SN63 alloy, indicating the improved corrosion resistance. Exposure of aluminum alloy to NaCl solution led to the formation of $Al(OH)_3/Al_2O_3$ which could be attributed to R_1 and Q_1 in the EC. Surface layer formed on the alloy

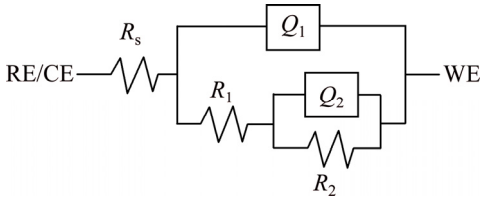

Fig. 6 Electrical equivalent circuit model used for curve fitting of EIS results (RE−Reference electrode; CE−Counter electrode; WE−Working electrode; R_s−Solution resistance; R_1−Surface layer resistance; R_2−Charge transfer resistance; Q_1−Constant phase element of surface layer; Q_2−Constant phase element of double layer)

Table 1 Equivalent circuit parameters of SN63 and SNC632 alloys

Parameter	SN63	SNC632
R_s/(Ω·cm²)	16.54±0.56	15.23±0.84
Q_1/(μS·s^n·cm^{-2})	147.0±30.2	131.2±19.4
n_1	0.922±0.03	0.927±0.02
R_1/(kΩ·cm²)	1.447±0.28	1.688±0.19
Q_2/(μS·s^n·cm^{-2})	907.1±145.2	833.1±152.3
n_2	0.973±0.04	0.899±0.06
R_2/(kΩ·cm²)	5.81±0.42	6.894±0.53
Error, χ^2	0.0008	0.0005

surface during exposure, and hence, R_1 is attributed to the surface layer resistance. Charge transfer between the surface layer and substrate is attributed to R_2 and Q_2. Increase of both R_1 and R_2 values of SNC632 alloy indicated the better surface and charge transfer (R_{ct}) resistance values compared to SN63 alloy.

Change in hydrogen volume as a function of time and comparison of corrosion rates after 72 h of exposure to NaCl solution are shown in Fig. 7. The volumes of hydrogen evolved for SN63 and SN632 alloys were found to be 0.13, 0.07 and 0.295, 0.16 mL/cm² after 24 and 72 h (Fig. 7(a)), respectively. These results confirmed that, the SNC632 alloy exhibited better corrosion resistance compared to the SN63 alloy. Corrosion rates measured by mass loss measurement (P_W) after 72 h were 0.15 and 0.08 mm/a for SN63 and SNC632 alloys, respectively. Corrosion rates measured using evolved hydrogen (P_H) also followed the similar trend and are in agreement with mass loss test. Addition of Cu decreased the corrosion rates confirming its beneficial role. The presence of single phase Cu at the grain boundary could minimize the influence of Al_3Ni phase, thereby improving the corrosion resistance. Addition of lower amount of Cu to Al alloy could dissolve and act as solute, and this further enhanced the corrosion resistance [30,31].

Macroscopic images of SN63 and SNC632 alloys after 72 h of exposure to NaCl solution are shown in Fig. 8 before and after removing the corrosion products.

It is visible from the macroscopic images that, white corrosion products were noticed on both the SN63 and SNC632 alloys after 72 h of exposure. Interestingly, the corrosion products appearing on SNC632 alloys are substantially less, indicating its better performance. No visible deep corrosion damages were noticed for both the SN63 and SNC632 alloys even after removing corrosion products. Corrosion morphologies and chemical composition of surface layer forming onto alloy were observed through FE-SEM and EDAX. Figures 9(a) and (b) show the corrosion morphologies of SN63 and SNC632 alloys, respectively. The surface covered with nodular like layers consisting of flake-like morphology was noticed on both SN63 and SNC632 alloys. The density of the surface layer was found to be larger for the SNC632 compared to the SN63 alloy. Elemental distribution of Al and O and the EDAX elemental composition are also depicted in Fig. 9. It is confirmed from the results that, the Al:O molar ratio was about 2:3 on both SN63 and SNC632 alloys, indicating that the surface layer mainly consisted of Al_2O_3. It is identified that, the surface layer forming on SNC632 alloy was relatively intact, which could control the penetration of aggressive ions, and thus possessed better resistance. It has been confirmed from the microstructures that Cu and Si have been precipitated at grain boundaries along with Al_3Ni phase as a continuous phase, which would also be responsible for the formation of stable surface layer [32].

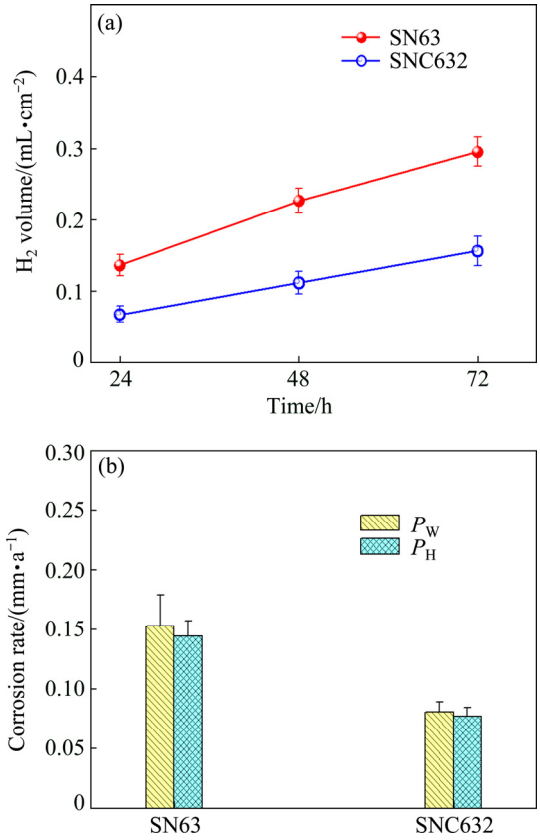

Fig. 7 Change in hydrogen volume as function of time (a) and comparison of corrosion rates (b) of SN63 and SNC632 alloys after 72 h of immersion in 3.5% NaCl solution

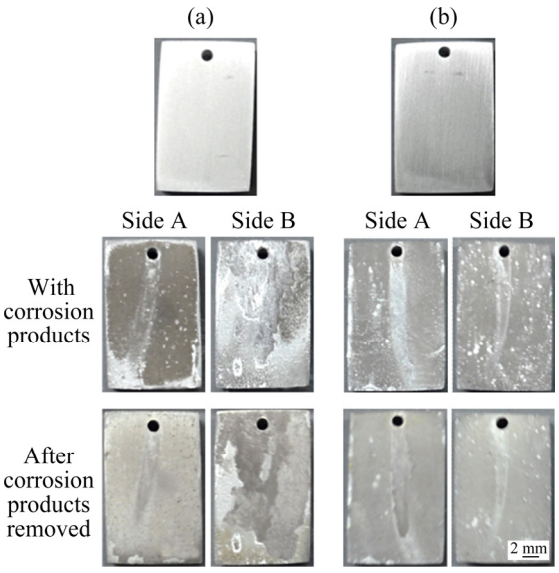

Fig. 8 Macroscopic images of SN63 (a) and SNC632 (b) alloys after 72 h of immersion in 3.5% NaCl solution

Figures 10(a) and (b) show the surface morphologies and elemental distributions after removing corrosion products of SN63 and SNC632 alloys, respectively. After 72 h of immersion, the secondary phases remained on the alloy surface and selective dissolution of α(Al) matrix has been confirmed. Cathodic nature of Al_3Ni/Al_3Ni_2 phases is responsible for the dissolution of Al matrix [24,27]. EDAX elemental distribution results also confirmed the precipitates at the grain boundary, which are nobler than the α(Al) matrix.

4 Conclusions

1) The presence of Al_3Ni phases and single Si phase was confirmed at the grain boundaries of SN63 alloy. Cu addition did not produce any additional Al-contained phases and the presence of Cu as solute at the grain boundaries was also noticed for SNC632 alloy. Besides, Cu addition resulted in the formation of Al_3Ni_2 phase. Microstructural studies further confirmed that, the precipitates were continuous at the grain boundaries.

2) Potentiodynamic polarization studies confirmed the lower J_{corr} value for the SNC632 compared to the SN63 alloy, which was attributed to the presence of solute Cu and Si phases along the grain boundaries as continuous phase, and this resulted in the formation of intact surface corrosion product layer.

3) Electrochemical impedance spectroscopy and equivalent circuit curve fitting analysis revealed the two-time constants behavior corresponding to

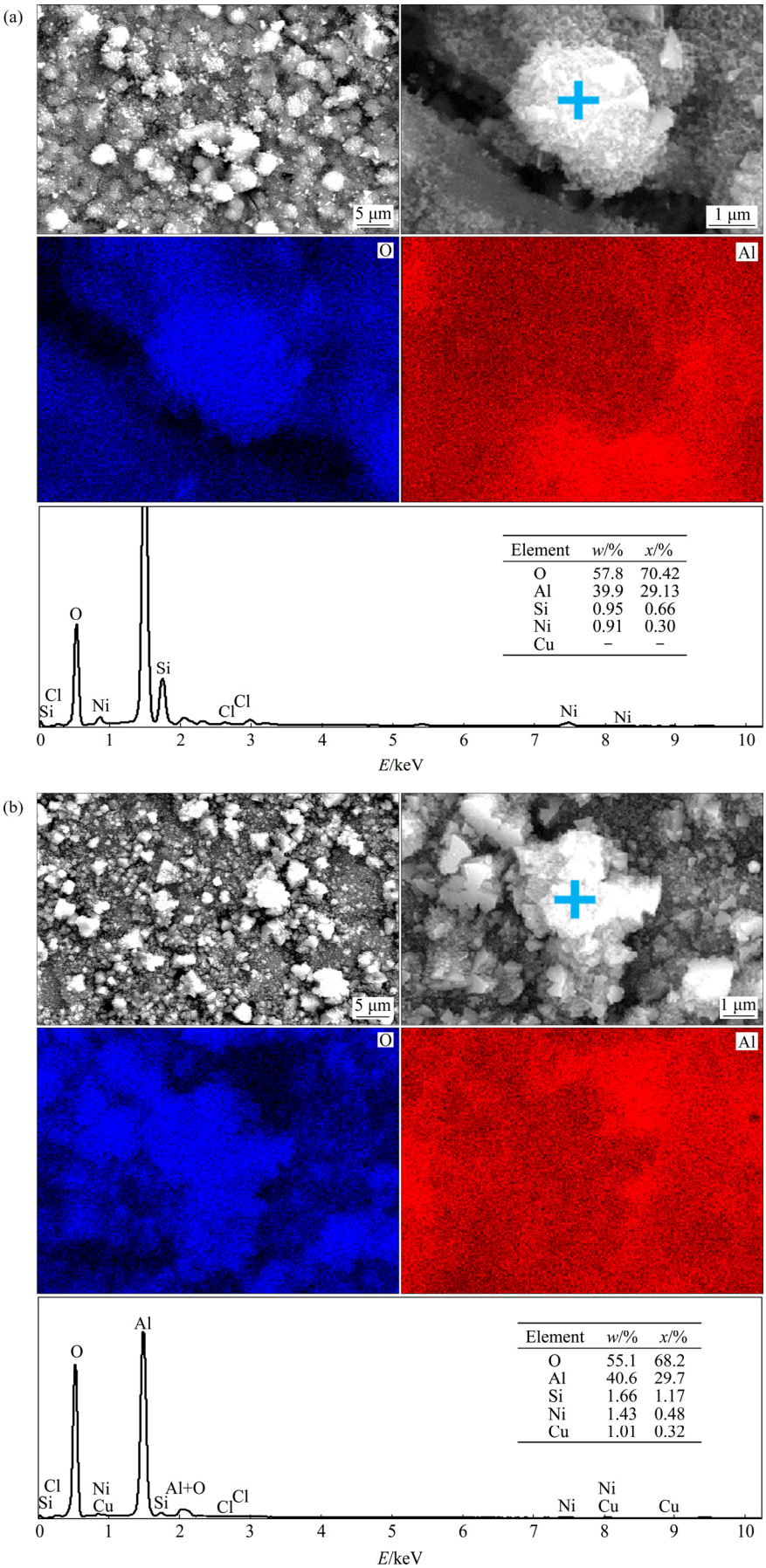

Fig. 9 Surface morphologies and EDAX elemental composition of SN63 (a) and SNC632 (b) alloys after 72 h of immersion with corrosion products

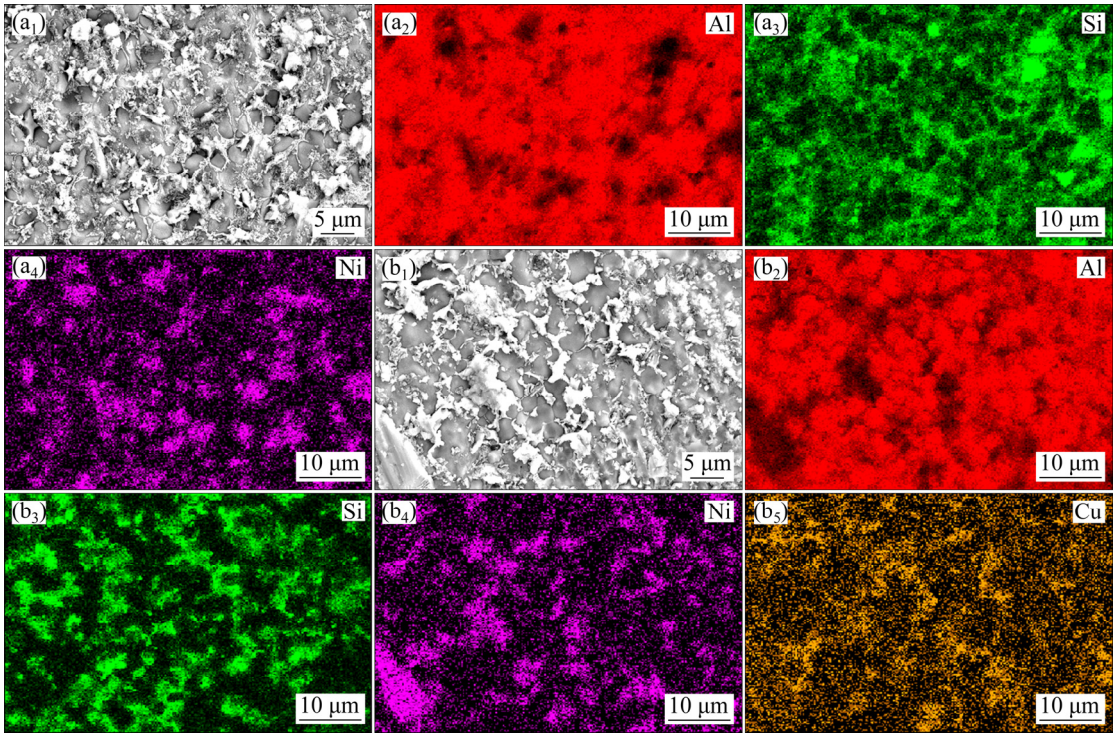

Fig. 10 Surface morphologies and EDAX elemental distributions after removing corrosion products of SN63 (a) and SNC632 (b) alloys after 72 h of immersion

electrolyte/surface layer and surface layer/substrate interfaces with larger surface layer and charge transfer resistance for the SNC632 alloy.

4) Immersion corrosion test results revealed the lower hydrogen volume and mass loss corrosion rates for the SNC632 alloy compared to the SN63 alloy. These results further substantiated the electrochemical corrosion results.

5) Corrosion product layers mainly consisted of Al_2O_3 layer after 72 h of exposure and surface layer was intact on SNC632 alloy. The selective dissolution of α(Al) matrix was confirmed after removing the corrosion products, and Al_3Ni/Al_3Ni_2, single phase Si and Cu also remained at grain boundaries. Hence, Cu addition played a beneficial role in improving the corrosion resistance of SN63 alloy.

Acknowledgements

This work was financially supported by the World Class 300 R&D Program (S2404600) funded by the Small Business Administration of Korea through the Research Institute of Advanced Materials (0417-20170037) and Magnesium Technology Innovation Center.

References

[1] RANA R S, PUROHIT R, DAS S. Reviews on the influences of alloying elements on the microstructure and mechanical properties of aluminum alloys and aluminum alloy composites [J]. International Journal of Scientific and Research, 2012, 2(6): 1−7.

[2] GAO Guan-jun, HE Chen, LI Yong, LI Jia-dong, WANG Zhao-dong, MISRA R D K. Influence of different solution methods on microstructure, precipitation behavior and mechanical properties of Al−Mg−Si alloy [J]. Transactions of Nonferrous Metals Society of China, 2018, 28(5): 839−847.

[3] SHI Yun-jia, PAN Qing-lin, LI Meng-jia, LIU Zhi-ming, HUANG Zhi-qi. Microstructural evolution during homogenization of DC cast 7085 aluminum alloy [J]. Transactions of Nonferrous Metals Society of China, 2015, 25(11): 3560−3568.

[4] SO T I, JUNG H C, LEE C D, SHIN K S. Effects of T6-treatment on the defect susceptibility of tensile strength to microporosity variation in low pressure die-cast A356 alloy [J]. Metals and Materials International, 2015, 21(5): 842−849.

[5] DAS S, MONDAL D P, SAWLA S, RAMKRISHNAN N. Synergic effect of reinforcement and heat treatment on the two body abrasive wear of an Al−Si alloy under varying loads and abrasive sizes [J]. Wear, 2008, 264: 47−59.

[6] ZAMANI M, SEIFEDDINE S, JARFORS A E W. High temperature tensile deformation behavior and failure mechanisms of an Al−Si−Cu−Mg cast alloy−The microstructural scale effect [J]. Materials & Design, 2015, 86: 361−370.

[7] ROBERGE P. Handbook of corrosion engineering [M]. New York: McGraw-Hill, 2000.

[8] OYA Y, KOJIMA Y, Hara N. Influence of silicon on intergranular corrosion for aluminum alloys [J]. Materials Transactions, 2013, 54(7): 1200−1208.

[9] CESCHINI L, MORRI A, MORRI A, TOSCHI S, JOHANSSON S, SEIFEDDINE S. Effect of microstructure and over aging on the tensile behavior at room and elevated temperature of C355-T6 cast aluminum alloy [J]. Materials & Design, 2015, 83: 626−634.

[10] DAVIS J R. Aluminum and aluminum alloys [M]. Metals Handbook Desk Edition. 2nd ed. ASM International, 1998: 417−505.

[11] MENDEZ F H, TORRES A A, HERNANDEZ J G M, ROJAS E T, RANGEL E R. Effect of nickel addition on microstructure and mechanical properties of aluminum-based alloys [J]. Materials Science Forum, 2011, 691: 10−14.
[12] SAKAMOTO Y, KAZITA N, SANUKI S, MAE T, NOTOYA H, ARAI K. Effect of Ni content on mechanical strength of improved Al−Mg (5052) alloys with Ni added by electron beam alloying [J]. Journal of the Japan Institute of Metals and Materials, 1999, 63(10): 1348−1355.
[13] OSORIO W R, SPINELLI J E, AFONSO C R M, PEIXOTO L C, GARCIA A. Electrochemical corrosion behavior of gas atomized Al−Ni alloy powders [J]. Electrochimica Acta, 2012, 69: 371−378.
[14] PERIC B, GRUBAC Z, SABLIC L. Studies of corrosion resistance of passive layers on Al−Ni alloys in the presence of chloride ions [J]. Croatica Chemica Acta, 1994, 67: 289−296.
[15] ZHAO W T, YAN D S, RONG L J. Influence of the Nickel on the corrosion behavior of Al−Mg−Sc−Zr alloy [J]. Materials Science Forum, 2007, 546−549: 1123−1128.
[16] OSORIO W R, PEIXOTO L C, CANTE M V, GARCIA A. Electrochemical corrosion characterization of Al−Ni alloys in a dilute sodium chloride solution [J]. Electrochimica Acta, 2010, 55: 4078−4085.
[17] WEN J, CUI H, WEI N, SONG X, ZHANG G, WANG C. Effect of phase composition and microstructure on the corrosion resistance of Ni−Al intermetallic compounds [J]. Journal of Alloys and Compounds, 2017, 695: 2424−2433.
[18] DIETER G E, BACON D J. Mechanical metallurgy [M]. Vol. 3. New York: McGraw-Hill, 1986.
[19] SHABESTARI S, MOEMENI H. Effect of copper and solidification conditions on the microstructure and mechanical properties of Al−Si−Mg alloys [J]. Journal of Materials Processing Technology, 2004, 153: 193−198.
[20] SEIFEDDINE S, SJOLANDER E, BOGDANOFF T. On the role of copper and cooling rates on the microstructure, defect formations and mechanical properties of Al−Si−Mg alloys [J]. Materials Sciences and Applications, 2013, 4: 171−178.
[21] ARTHANARI S, JANG J C, SHIN K S. Corrosion studies of high pressure die-cast Al−Si−Ni and Al−Si−Ni-Cu alloys [J]. Journal of Alloys and Compounds, 2018, 749: 146−154.
[22] ARTHANARI S, JANG J C, SHIN K S. Corrosion behavior of high pressure die-cast Al−Ni and Al−Ni−Ca alloys in 3.5% NaCl solution [J]. Corrosion Science and Technology, 2017, 16(3): 100−108.
[23] YU P, DENG C J, MA N G, M. YAU Y, NG D H L. Formation of nanostructured eutectic network in α-Al_2O_3 reinforced Al−Cu alloy matrix composite [J]. Acta Materialia, 2003, 51(12): 3445−3454.
[24] OSORIO W R, MOUTINHO D J, PEIXOTO L C, FERREIRA I L, GARCIA A. Macrosegregation and microstructure dendritic array affecting the electrochemical behaviour of ternary Al Cu Si alloys [J]. Electrochimica Acta, 2011, 56: 8412−8421.
[25] OSORIO W R, PEIXOTO L C, MOUTINHO D J, GOMES L G, FERREIRA I L, GARCIA A. Corrosion resistance of directionally solidified Al−6Cu−1Si and Al−8Cu−3Si alloys castings [J]. Materials and Design, 2011, 32: 3832−3837.
[26] OSORIO W R, SIQUEIRA C A, SANTOS C A, GARCIA A. The correlation between electrochemical corrosion resistance and mechanical strength of as-cast Al−Cu and Al−Si alloys [J]. International Journal of Electrochemical Science, 2011, 6: 6275−6289.
[27] OSORIO W R, FREITAS E S, SPINELLI J E, CANTE M V, AFONSO C R M, GARCIA A. Assessment of electrochemical and mechanical behavior of hot-extruded powders and as-cast samples of Al−Ni alloys [J]. International Journal of Electrochemical Science, 2012, 7: 9946−9971.
[28] JIA J X, ATRENS A, SONG G, MUSTER T H. Simulation of galvanic corrosion of magnesium coupled to a steel fastener in NaCl solution [J]. Materials and Corrosion, 2005, 56: 468−474.
[29] LIANG W J, ROMETSCH P A, CAO L F, BIRBILIS N. General aspects related to the corrosion of 6xxx series aluminum alloys: Exploring the influence of Mg/Si ratio and Cu [J]. Corrosion Science, 2013, 76: 119−128.
[30] LITTLE D A, CONNOLLY B J, SCULLY J R. An electrochemical framework to explain the intergranular stress corrosion behavior in two Al−Cu−Mg−Ag alloys as a function of aging [J]. Corrosion Science, 2007, 49: 347−372.
[31] ABURADA T, UNLU N, FITZ-GERALD J M, SHIFLET G J, SCULLY J R. Effect of Ni as a minority alloying element on the corrosion behavior in Al−Cu−Mg− (Ni) metallic glasses [J]. Scripta Materialia, 2008, 58: 623−626.

高压铸造 Al−6Si−3Ni 及 Al−6Si−3Ni−2Cu 合金在 NaCl 水溶液中的抗腐蚀性能

Srinivasan ARTHANARI, Jae Cheol JANG, Kwang Seon SHIN

Research Institute of Advanced Materials, School of Materials Science and Engineering,
Seoul National University, Gwanak-gu, Seoul 08826, Korea

摘　要：研究高压铸造 Al−6Si−3Ni(SN63)及 Al−6Si−3Ni−2Cu(SNC632)合金在 3.5%(质量分数)NaCl 水溶液中的腐蚀行为。X 射线衍射及显微组织分析表明，单相 Si 及 Al_3Ni/Al_3Ni_2 二元相分布在合金的晶界处，并且在 SNC632 合金晶界处析出单相 Cu。电化学腐蚀实验结果表明，与 SN63 合金相比，SNC632 合金表现出高的腐蚀电位(φ_{corr})，低的腐蚀电流密度(J_{corr})及高的耐腐蚀性。电化学阻抗谱(EIS)等效电路曲线拟合分析表明，电解质与衬底之间存在两个界面，而 SNC632 合金的电荷转移电阻(R_{ct})要比 SN63 合金的高。浸泡腐蚀试验与电化学腐蚀结果一致，SNC632 合金表现出较高的耐腐蚀性。Cu 元素的添加导致在 SNC632 合金并未出现含金属间化合物的次生铜相而出现单相 Cu，进而提高其抗腐蚀性。

关键词：压铸；铝合金；腐蚀；极化；电化学阻抗谱

(Edited by Bing YANG)